Forest Ecology and Management 292 (2013) 75–85

Contents lists available at SciVerse ScienceDirect

Forest Ecology and Management

journal homepage: www.elsevier.com/locate/foreco

Strategies for minimizing sample size for use in airborne LiDAR-based forest inventory

Virpi Junttila [a,*], Andrew O. Finley [b], John B. Bradford [c], Tuomo Kauranne [a]

[a] Department of Applied Mathematics, Lappeenranta University of Technology, Lappeenranta, Finland
[b] Departments of Forestry and Geography, Michigan State University, East Lansing, MI, USA
[c] U.S. Geological Survey, Southwest Biological Science Center, Flagstaff, AZ, USA

ARTICLE INFO

Article history:
Received 17 October 2012
Received in revised form 13 December 2012
Accepted 17 December 2012

Keywords:
Optimal design
Geostatistical
LiDAR
Bayesian
Biomass

ABSTRACT

Recently airborne Light Detection And Ranging (LiDAR) has emerged as a highly accurate remote sensing modality to be used in operational scale forest inventories. Inventories conducted with the help of LiDAR are most often model-based, i.e. they use variables derived from LiDAR point clouds as the predictive variables that are to be calibrated using field plots. The measurement of the necessary field plots is a time-consuming and statistically sensitive process. Because of this, current practice often presumes hundreds of plots to be collected. But since these plots are only used to calibrate regression models, it should be possible to minimize the number of plots needed by carefully selecting the plots to be measured. In the current study, we compare several systematic and random methods for calibration plot selection, with the specific aim that they be used in LiDAR based regression models for forest parameters, especially above-ground biomass. The primary criteria compared are based on both spatial representativity as well as on their coverage of the variability of the forest features measured. In the former case, it is important also to take into account spatial auto-correlation between the plots. The results indicate that choosing the plots in a way that ensures ample coverage of both spatial and feature space variability improves the performance of the corresponding models, and that adequate coverage of the variability in the feature space is the most important condition that should be met by the set of plots collected.

1. Introduction

Prediction of forest variables, with associated uncertainty, at a fine spatial resolution over large domains is used to inform forest management and policy decisions, further environmental research, and to serve as base data for a range of environmental monitoring initiatives. For instance, several multinational initiatives include specific requirements for spatially explicit estimates of forest biomass – a proxy for carbon – with specific levels of accuracy. Two notable initiatives include the U.N. Framework Convention on Climate Change Kyoto Protocol and, more recently, the REDD+ program mandated by the Climate Conference in Durban in 2011. Additionally, several National Forest Inventory (NFI) programs have adapted their inventory and analysis to better support reporting and research on carbon budgets via forest biomass estimation.

Multisource forest inventory methods couple georeferenced forest inventory field plot measurements with remotely sensed data, most commonly in the form of remotely sensed imagery or more recently Light Detection And Ranging (LiDAR), to improve large- and small-scale prediction of forest variables. Many studies, some of which are noted below, have detailed such methods to improve prediction and mapping of forest biomass and other important economic and ecological forest variables.

While remote sensing based methods, such as the ones listed above, are cost-effective and accurate, they require a representative field sample for calibrating their parameters. Such methods are most often model-based, or Bayesian, in character. Among these methods, recently especially LiDAR has gained in popularity, to the extent that some countries, including Finland (Maltamo et al., 2011b), have chosen it as the only method to be used in medium-scale operational forest inventory. By medium-scale we mean the case where inventories are produced at stand level over a total forest area of at most a million hectares in size. In national scale inventory, over several millions of hectares of forestland, satellite image based methods are still the best choice, because of the low cost and temporally high frequency of satellite imagery. The main disadvantage of using satellite images is a precision and spatial resolution that are both significantly weaker than when LiDAR is used. In this article, our focus is on medium-scale forest inventory.

Motivated by a need to produce cost effective assessments of forest variables using a combination of field measurements and remotely sensed data, we explore approaches to minimizing the number of forest inventory plots visited while maximizing predic-

* Corresponding author. Tel.: +358 50 331 6465; fax: +358 5 621 2350.
E-mail address: virpi.junttila@lut.fi (V. Junttila).

0378-1127/$ - see front matter © 2012 Elsevier B.V. All rights reserved.
http://dx.doi.org/10.1016/j.foreco.2012.12.019

tive performance and minimizing bias. We focus on characterizing the impact of sampling intensity and design on measures of forest variables along with estimates of uncertainty for arbitrarily defined areas of interest.

A variety of multisource forest inventory methods are common in the literature, including non-parametric approaches such as k-nearest neighbor and Random Forest (see, e.g., McRoberts (2012), and references there in) and parametric regression and geostatistical approaches. Geostatistical approaches such as kriging and cokriging (see, e.g., Cressie (1993), Chilés and Delfiner (1999), Banerjee et al. (2004)) have been used extensively to improve prediction and quantify uncertainty (see, e.g., Hudak et al. (2002), Finley et al. (2008a), Finley et al. (2008b), Finley et al. (2009), Finley et al. (2011)).

All multisource methods attempt to improve inference by exploiting the relationship between the forest variable of interest, referred to as the response variable, and the remotely sensed variables, referred to as the covariates. If this relationship is strong and the postulated model is able to capitalize on this relationship, then substantial gains in efficiency can be realized. Here, we define *efficiency* in terms of the model's predictive accuracy and precision given a fixed number of forest inventory plot observations. We also note that efficiency is a function of the number of observations, their information content, and the postulated model.

When considering sampling designs for use in multisource model-based inventories, a common objective is to approximate complete coverage of the domain by placing plots on a regular grid, or randomly within regular polygons that tesselate the area of interest, see, e.g., Paciomik and Rypdal (2003) and McRoberts et al. (2005). Additionally, some prior knowledge about the forest characteristics, such as forest type, forest land use history, or information estimated from remotely sensed data, can be used to improve the design (Means et al., 1999; Brown, 2002; Patenaude et al., 2004). However, these approaches do not explicitly consider the relationship between the forest response variable and remotely sensed covariates used in the postulated model, and therefore miss an opportunity to gain efficiency.

Several studies have found a strong correlation between remotely sensed covariates, in particular those derived from LiDAR, and forest response variables, see, e.g., Næsset (1997), Means et al. (1999), Rooker Jensen et al. (2006), Magnussen et al. (2010). In such cases, the variability and spatial distribution of the forest variables can be reasonably well estimated using the LiDAR covariates, even in the absence of field sampling. If these same relationships exist in *new* inventory areas, then the readily available LiDAR covariates can be used as auxiliary data, in conjunction with the postulated model, to guide selection of inventory plot locations to maximize information gain and hence efficiency.

The relationship between sample design and model-based inference in multisource inventory settings has been partially explored in several recent studies. Junttila et al. (2008) considered the effect of LiDAR covariates and varying intensities of inventory plots for predicting a host of forest variables using ordinary least-squares and Sparse Bayesian regression models. Hawbaker et al. (2009) assessed two sampling designs for informing a regression model used for predicting biomass and other forest variables. Here, field data were drawn from a simple random sample and stratified sample that was informed using mean and standard deviation of LiDAR canopy height estimates. In a similar study, that used a *k*-NN method to predict forest stand parameters, Maltamo et al. (2011a) considered several plot selection strategies including random selection, random selection within pre-stratification according to forest type, and selection of plots based on properties of the LiDAR data given as *a priori* information.

These studies showed that prediction error increases as the number of field sample plots diminishes; however, given auxiliary data in the form of LiDAR variables, and field sample plot selection criteria via stratification, good results can be achieved even with only a few dozen field sample plots. These studies did not explicitly leverage the postulated model to guide plot selection; rather, the plot selection utility function was somewhat arbitrary and disjoint from the modeling phase. Therefore, some questions remain. First, can we realize gains in efficiency when the postulated model and LiDAR data are both considered in the plot selection? Second, can we use *a priori* knowledge about a possible relationship between LiDAR covariates and the forest response variable to preferentially select plot locations to sample? The answer to the first question is likely *yes* in most settings, however, preferential selection of inventory plots can also result in biased prediction. Therefore, for this result to be useful in application, we need to be able to say something about the amount of bias in the subsequent prediction. Third, are the answers to the first and second questions consistent across sites?

In this study, three different selection criteria based on LiDAR data and/or plot location are considered for inventory plot selection at three distinct study sites. Our interest is in maintaining the robustness of prediction even under a severe reduction in the number of plots measured. In particular, we consider gains in efficiency versus introduction of bias. To simulate a realistic multisource inventory of a *new* study site, all the selection criteria use only covariates estimated from the sites' LiDAR data, i.e., the criteria do not use information from forest variables measured at the study sites.

The remainder of the paper is organized as follows: Section 2 details the proposed selection criteria and candidate models. Section 3 describes the study sites, associated data, and analysis. Analysis results and discussion is offered in Section 4. Finally, a summary with an indication toward future work are provided in Section 5.

2. Methods

Let us assume the forested domain can be partitioned into N fixed area plots that comprise the inventory sample frame. A set of variables, potentially estimated from remotely sensed data, is available for each plot and stored in a $p \times 1$ vector $\boldsymbol{x}_i$ along with an intercept of constant value 1, where i indexes the plots $i = 1, \ldots, N$. These variables, which will serve as the covariates in the subsequent regression model, are collected into a $N \times p$ matrix $\boldsymbol{X}$, i.e., $\boldsymbol{x}_i'$ is the ith row of $\boldsymbol{X}$. In addition to the covariates, the centroid coordinates, i.e., easting and northing, for each plot are known and stored in a 2×1 vector $\boldsymbol{s}_i$, where again i indexes the plot. Similar to the covariates, these coordinates are organized into a $N \times 2$ matrix $\boldsymbol{S}$. For the current setting, only the plot covariates and centroid coordinates are known. In the subsequent development we refer to these data as the auxiliary data.

From the N plots available in the domain, $n \leqslant N$ plots are selected into the sample using a criterion defined in Section 2.1. To keep track of which plots are selected into the sample, we define a design vector $\boldsymbol{f}$ of length n that holds the sample plots' index in the sample frame, i.e., each element $\boldsymbol{f}_j$, $j = 1, \ldots, n$, is a distinct plot index that references a plot in the sample frame, $\boldsymbol{f}_j \in \{1, \ldots N\}$.

Given a design vector, $\boldsymbol{f}$, the n sample plots are visited and corresponding forest variable measurements are recorded. These measurements are stored in a $n \times 1$ vector $\boldsymbol{y}_{\boldsymbol{f}}$, which serves as the response vector in the subsequent regression. The design vector is also used to select rows in matrices $\boldsymbol{X}$ and $\boldsymbol{S}$ to form $\boldsymbol{y}_{\boldsymbol{f}}$'s corresponding $n \times p$ $\boldsymbol{X}_{\boldsymbol{f}}$ and $n \times 2$ $\boldsymbol{S}_{\boldsymbol{f}}$ matrices. The regression model is written as follows

$$\boldsymbol{y}_{\boldsymbol{f}} = \boldsymbol{X}_{\boldsymbol{f}}\boldsymbol{\beta} + \boldsymbol{w}_{\boldsymbol{f}} + \boldsymbol{\epsilon}, \tag{1}$$

where $\boldsymbol{\beta}$ is a $p \times 1$ vector of regression coefficients, $\boldsymbol{w}_{\boldsymbol{f}}$ is a $n \times 1$ vector of spatial random effects, and $\boldsymbol{\epsilon}$ is a $n \times 1$ vector of residuals. The

spatial random effects arise from a Multivariate Normal (MVN), $MVN(\mathbf{0},\mathbf{C_f}(\boldsymbol{\eta}))$, where the (i,j)th element of the $n \times n$ covariance matrix $\mathbf{C_f}(\boldsymbol{\eta})$ is $\sigma^2\rho(\boldsymbol{s}_i, \boldsymbol{s}_j; \phi)$ and $\boldsymbol{\eta} = \{\sigma^2, \phi\}$. Here we choose to work with the Exponential correlation function, such that $\rho(\boldsymbol{s}_i, \boldsymbol{s}_j;\phi) = \exp(-\phi\|\boldsymbol{s}_i - \boldsymbol{s}_j\|)$, ϕ is considered the spatial decay parameter, and $\|\boldsymbol{s}_i - \boldsymbol{s}_j\|$ is the euclidean distance between plot locations $\boldsymbol{s}_i$ and $\boldsymbol{s}_j$. Other *valid* spatial correlation functions could be considered, see, e.g., Cressie (1993). The vector $\boldsymbol{\epsilon}$ follows a $MVN(\mathbf{0}, \tau^2 I_n)$ with scalar variance τ^2 and $n \times n$ identity matrix I_n, i.e., independent and identically distributed residuals.

To reduce the dimension of the parameter space, we integrate over the spatial random effects and work with the marginalized likelihood of (1), $\boldsymbol{y_f} \sim MVN(\boldsymbol{X_f\beta}, \boldsymbol{\Sigma_f}(\theta))$ where $\boldsymbol{\Sigma_f}(\theta) = \mathbf{C_f}(\boldsymbol{\eta}) + \tau^2 I_n$ and $\theta = \{\tau^2, \sigma^2, \phi\}$. The estimates for θ, denoted $\hat{\theta}$, were obtained using an efficient Markov chain Monte Carlo (MCMC) algorithm under a Bayesian formulation, see, Finley and Banerjee (2012) for additional details.

As described in Section 1, we would like to base comparisons on *efficiency* defined in terms of predictive accuracy and precision. Hence, we are interested in making predictions for those plots in the sample frame that are not indexed in $\boldsymbol{f}$. We denote this $N - n$ complement set index vector as $\boldsymbol{v}$ and refer to it as the verification set. Similar to our use of $\boldsymbol{f}$, the verification index vector is used to subset $\boldsymbol{X}$ and $\boldsymbol{S}$ to form the $(N-n) \times p$ $\boldsymbol{X_v}$ and $(N-n) \times 2$ $\boldsymbol{S_v}$ matrices.

Following from (1), the predictive distribution for the jth plot indexed in $\boldsymbol{v}$ is $\hat{y}_j \sim N\left(\boldsymbol{\mu}_{\boldsymbol{y},j}, \boldsymbol{\tau}^2_{\boldsymbol{y},j}\right)$, where

$$\boldsymbol{\mu}_{\boldsymbol{y},j} = \boldsymbol{x}_j\hat{\boldsymbol{\beta}} + \boldsymbol{c}_j(\hat{\boldsymbol{\eta}})'\boldsymbol{\Sigma_f}(\hat{\theta})^{-1}(\boldsymbol{y_f} - \boldsymbol{X_f}\hat{\boldsymbol{\beta}}), \tag{2}$$

$$\boldsymbol{\tau}^2_{\boldsymbol{y},j} = \hat{\tau}^2 - \boldsymbol{c}_j(\hat{\boldsymbol{\eta}})'\boldsymbol{\Sigma_f}(\hat{\theta})^{-1}\boldsymbol{c}_j(\hat{\boldsymbol{\eta}}) + \boldsymbol{\Delta x}'_j\left(\boldsymbol{X}'_{\boldsymbol{f}}\boldsymbol{\Sigma_f}(\hat{\theta})^{-1}\boldsymbol{X_f}\right)^{-1}\boldsymbol{\Delta x}_j, \tag{3}$$

$\boldsymbol{x}_j$ is the jth row of matrix $\boldsymbol{X_v}$, $\boldsymbol{c}_j(\hat{\boldsymbol{\eta}})$ is the $n \times 1$ vector of covariances between plot location $\boldsymbol{s}_j$ and locations $\boldsymbol{S_f}$, $\hat{\boldsymbol{\beta}}$ is the vector of estimated regression coefficients, and $\boldsymbol{\Delta x}_j = \boldsymbol{x}_j - \boldsymbol{c}_j(\hat{\boldsymbol{\eta}})'\boldsymbol{\Sigma_f}(\hat{\theta})^{-1}\boldsymbol{X_f}$. This result is also known as the universal Kriging variance, see e.g. Christensen (1990). One can obtain $\hat{\boldsymbol{\beta}}$ from the MCMC algorithm noted previously, or, given $\hat{\theta}$, compute $\hat{\boldsymbol{\beta}} = \left(\boldsymbol{X}'_{\boldsymbol{f}}\boldsymbol{\Sigma_f}(\hat{\theta})^{-1}\boldsymbol{X_f}\right)^{-1}\boldsymbol{X}'_{\boldsymbol{f}}\boldsymbol{\Sigma_f}(\hat{\theta})^{-1}\boldsymbol{y_f}$.

2.1. Design criteria

There are several strategies for choosing an *optimal* design vector $\boldsymbol{f}^*$. Here, we consider two general approaches. The first, referred to as a *space filling design*, attempts to sample uniformly across a feature space. In our setting, the feature space can be defined using geographic coordinates or a coordinate system derived from the covariates. The second considers qualities of the postulated model (1) and attempts to minimize some function of prediction error. Both approaches can be used to define an objective function $u(\boldsymbol{f})$. Then, given a fixed sample size n, the optimal design vector is found by solving the optimization (minimization) problem $\boldsymbol{f}^* = \text{arg}\min_{\boldsymbol{f}} u(\boldsymbol{f})$. A solution to this problem requires a potentially computationally intensive search among specification of $\boldsymbol{f}$.

2.1.1. Space filling design

The Maximin design, e.g., detailed in Morris and Mitchell (1995) and Trosset (1999), is a space filling design that attempts to cover a feature space as uniformly as possible given a fixed number of points, i.e., sample size in our case. The Maximin utility function maximizes the minimal distance between plots, or equivalently minimizes its negative or inverse value.

Consider some generic feature space that is associated with the sample frame and defined by a $N \times q$ matrix $\boldsymbol{Z}$. Here q refers to the arbitrary number of variables in $\boldsymbol{Z}$. The squared Euclidean distance between row i and j of $\boldsymbol{Z}$ is $d(i,j) = \sum_{k=1}^{q}(\boldsymbol{Z}_{i,k} - \boldsymbol{Z}_{j,k})^2$. Then, given this definition, the Maximin design utility function is

$$u_{m,\boldsymbol{Z}}(\boldsymbol{f}) = \frac{1}{\min d(i,j)}, \; i,j \in \boldsymbol{f} \text{ and } i \neq j, \tag{4}$$

where m refers fo "Maximin", and i and j are two distinct plots included in $\boldsymbol{f}$. If $\boldsymbol{Z} = \boldsymbol{S}$, minimization of $u_{m,\boldsymbol{S}}(\boldsymbol{f})$ will produce a $\boldsymbol{f}^*$ that identifies sample plots that cover the domain as uniformly as possible. For example, if $\boldsymbol{S}$ defines a dense grid over the domain, then minimization of this utility function results in an approximately regular grid of n plots over the domain. Alternatively, one could set $\boldsymbol{Z} = \boldsymbol{X}$, then minimization of $u_{m,\boldsymbol{X}}(\boldsymbol{f})$ will produce a $\boldsymbol{f}^*$ that identifies sample plots that cover the covariate space as uniformly as possible.

2.1.2. Designs minimizing linear prediction error variance

Instead of specifying a sampling design using only information in the auxiliary data feature space, it might be more fruitful to consider the predictive distribution of the postulated model. In fact, this seems more natural, or direct, given that our objective is to improve predictive accuracy and precision. The challenge is that only the auxiliary data are known *a priori* and without response variable measurements the model parameters cannot be estimated and hence the predictive distribution cannot be fully specified. However, as detailed below, given some "reasonable" estimate of θ some gains in efficiency might be realized.

Classical optimal designs for linear models are discussed, e.g. in Silvey (1980) and Atkinson and Donev (1992), where optimality refers to minimizing model parameters' error variance–covariance or maximizing some measure of information gain. In our setting, interest is in specifying a design that leads to optimal prediction of a forest response variable, therefore we seek the design that minimizes the prediction error variance. The prediction error variance for (1), given in (3), depends on the auxiliary data and parameters associated with the spatial random effects and residuals, not on the response variable measurements. Thus, given n, $\boldsymbol{X}$, $\boldsymbol{S}$, and estimates of $\boldsymbol{\theta}$, the postulated model can help inform plot selection into the sample – before response measurements are collected.

It turns out that the first component in (3), the τ^2 parameter often referred to as the *nugget* or *pure error* variance, affects the prediction error variance only as a constant and can therefore be ignored when comparing among different designs. Thus, we might consider the prediction error utility function

$$u_{\text{lin},\theta}(\boldsymbol{f}) = (u_1 + u_2)/(N - n), \tag{5}$$

where

$$u_1 = -\text{trace}(\boldsymbol{c_v}(\boldsymbol{\eta})'\boldsymbol{\Sigma_f}(\boldsymbol{\theta})^{-1}\boldsymbol{c_v}(\boldsymbol{\eta})), \tag{6}$$

$$u_2 = \text{trace}\left(\boldsymbol{\Delta x}'_{\boldsymbol{v}}\left(\boldsymbol{X}'_{\boldsymbol{f}}\boldsymbol{\Sigma_f}(\boldsymbol{\theta})^{-1}\boldsymbol{X_f}\right)^{-1}\boldsymbol{\Delta x_v}\right) \tag{7}$$

and $\boldsymbol{\Delta x_v} = \boldsymbol{x_v} - \boldsymbol{c_v}(\boldsymbol{\eta})'\boldsymbol{\Sigma_f}(\boldsymbol{\theta})^{-1}\boldsymbol{X_f}$. This utility function is referred to as the Mean Universal Kriging variance in Brus and Heuvelink (2007). Collectively, u_1 and u_2 consider the distribution of sample plots in geographic space and covariate feature space. The utility function also accounts for the strength of spatial dependence, and hence attempts to reduce the amount of redundant information resulting from samples located *too* close together in geographic space. Specifically, a $\boldsymbol{f}^*$ that minimizes the utility function's first component, u_1, maximizes the geographic distance between sample plots and minimizes their distance to prediction plots indexed in $\boldsymbol{v}$. The strength of the spatial correlation, controlled by ϕ, dictates the influence of u_1 in the utility function. The utility function's second component, u_2, also contributes to plot separation in geographic space, given

the strength of the spatial correlation, but also attempts to select samples on or near the convex hull of the covariate space.

To more clearly understand the contribution of the utility function's components, it is helpful to consider the case where the spatial correlation among verification plot measurements is assumed to be zero, i.e., $\boldsymbol{c}_v(\eta) = \mathbf{0}$.

Here, the prediction variance utility function becomes

$$\text{trace}\left(\boldsymbol{X}_v\left(\boldsymbol{X}_f'\boldsymbol{\Sigma}_f^{-1}\boldsymbol{X}_f\right)^{-1}\boldsymbol{X}_v'\right), \tag{8}$$

and results in a $\boldsymbol{f}^*$ that minimizes $\boldsymbol{\beta}$'s covariance matrix, $\boldsymbol{\Sigma}_\beta = \left(\boldsymbol{X}_f'\boldsymbol{\Sigma}_f^{-1}\boldsymbol{X}_f\right)^{-1}$, weighted by the verification set's covariates. When each covariate column in $\boldsymbol{X}$ is scaled to the range $[-1, 1]$, the plots with covariate values close to $\{-1, 1\}$ are selected into the sample first. Thus the linear model is defined using the plots with extreme values of covariates. Hengl et al. (2003) apply this aspatial approach to determine sampling designs for soil surveys.

If spatial dependence among plot measurements is negligible, i.e., $1/\phi \to 0$, the model covariance matrix becomes diagonal, $\boldsymbol{\Sigma}_f = (\tau^2 + \sigma^2)\boldsymbol{I}_n$. In this case the constant scale term $(\tau^2 + \sigma^2)$ can be ignored (it does not influence comparison among utility function values) and the utility function (5) is reduced to

$$\text{trace}\left(\boldsymbol{X}_v\left(\boldsymbol{X}_f'\boldsymbol{X}_f\right)^{-1}\boldsymbol{X}_v'\right), \tag{9}$$

and only the covariate distribution influences the selection of $\boldsymbol{f}^*$.

The design vector obtained using (9) is known to be efficient and optimal only when the relationship between the response and covariates can be well approximated by the linear model. If the relationship between the covatiates and response is nonlinear, the design can lead to biased results. The addition of spatial dependence in (5) is an attempt to minimize this potential bias, while still realizing some of the advantages of covering the covariate feature space.

2.2. Simulated annealing

Given a utility function, the search for the optimal design vector $\boldsymbol{f}^*$ requires an intensive search among specifications of $\boldsymbol{f}$. This search becomes computationally onerous for even a moderately sized sample frame and sample size, e.g., $N = 100$ and $n = 25$ is $\binom{N}{n} = 75,287,520$ different $\boldsymbol{f}$'s must be evaluated. An alternative to the brute force search is to use an efficient search algorithm such as simulated annealing, see, e.g., Zhou (2008) and Fang and Wiens (2000).

The simulated annealing algorithm used in our study is as follows. Start with the *current* design vector, $\boldsymbol{f}_{\text{curr}}$ that, for the first iteration of the algorithm, comprises n randomly chosen plots which serve as initial values. A new candidate design vector is formed by setting $\boldsymbol{f}_{\text{cand}}$ equal to $\boldsymbol{f}_{\text{curr}}$ then replacing one index in $\boldsymbol{f}_{\text{cand}}$ with an index selected randomly from those $N - n$ plots remaining in the sample frame. Then $\boldsymbol{f}_{\text{cand}}$ is *accepted* if the utility function value $u(\boldsymbol{f}_{\text{cand}})$ is smaller than $u(\boldsymbol{f}_{\text{curr}})$, or $\exp(-(u(\boldsymbol{f}_{\text{cand}}) - u(\boldsymbol{f}_{\text{curr}}))/T) > \alpha$, where T is a cooling temperature specified by the user and α is a random variate drawn from a Uniform distribution with support from 0 to 1. If both conditions are not satisfied, then $\boldsymbol{f}_{\text{cand}}$ is *rejected*. When $\boldsymbol{f}_{\text{cand}}$ is accepted, it replaces $\boldsymbol{f}_{\text{curr}}$, otherwise, a new candidate design vector is formed from $\boldsymbol{f}_{\text{curr}}$ as described above. These steps continue until $\boldsymbol{f}_{\text{curr}}$ does not change for some prespecified number of iterations. For our study this threshold was 30,000 and the cooling temperature was reduced by 0.9 every 100 iterations. To ensure a stable solution to $\boldsymbol{f}^*$ was found, this algorithm was run multiple times using different initial design vectors and random number generator seeds.

3. Case studies

3.1. Forest inventory data

The sampling design criteria detailed in Section 2.1 were assessed using three forest inventory datasets that are part of the multiagency U.S. North American Carbon Program. Each dataset comprises point-referenced measures of above ground forest biomass and covariates derived from discrete LiDAR data. The datasets come from the Fraser Experimental Forest (FEF) located in central Colorado near the town of Fraser, Marcell Experimental Forest (MEF) located in northern Minnesota, and Niwot Long Term Ecological Research Site (NIWOT) on the front range of the Rocky Mountains, near the town of Nederland, Colorado.

Tree species at FEF consist primarily of *Abies lasiocarpa* and *Picea engelmannii* at higher elevations and *Pinus contorta* at lower elevations. Climate at FEF is characterized by cold and relatively long winters, with mean annual temperature and precipitation of 0 °C and 737 mm, respectively. MEF consists of mixed forests that include both upland forests and peat lands. Upland forests are generally dominated by *Populus tremuloides* and *grandidentata*, but contain substantial components of *Betula papyrifera, Pinus resinosa, Pinus strobus*, and *Pinus banksiana*. Lowland tree species include *Larix laricina*, *Picea mariana*, *Fraxinus nigra*, and *Thuja occidentalis*. Climate at MEF is sub-humid continental, with mean annual precipitation of 785 mm, mean annual temperature of 3 °C and air temperature extremes of −46 °C and 38 °C. Tree species in NIWOT include primarily a mix of *Abies lasiocarpa, Picea engelmannii* and *Pinus contorta* with minor components of *Pinus flexilis* and *Populus tremuloides*. Mean annual temperature and precipitation are 4 °C and 800 mm, respectively.

Field data at each site were collected using methods similar to the Forest Inventory and Analysis cluster plot design (Bechtold and Patterson, 2005). The cluster configuration consists of four 8–10 m radius plots (depending on the site) with one at the cluster center and the other three positioned 35 m away from the center at 0°, 120°, and 240°. Additional single plots were distributed throughout the site. FEF, MEF, and NIWOT contained 60, 99, and 62 plots respectively. Within each plot, tree diameter at breast height and height measurements for both live and dead trees were taken and used in species specific allometric models to estimate above ground biomass (AGB) including stem, branch, and foliage. Additional details about field measurements and allometric equations used for biomass estimation are available in Bradford et al. (2010). Plot level AGB in Mg/ha was calculated by summing individual tree estimates for each plot. The variability of AGB values

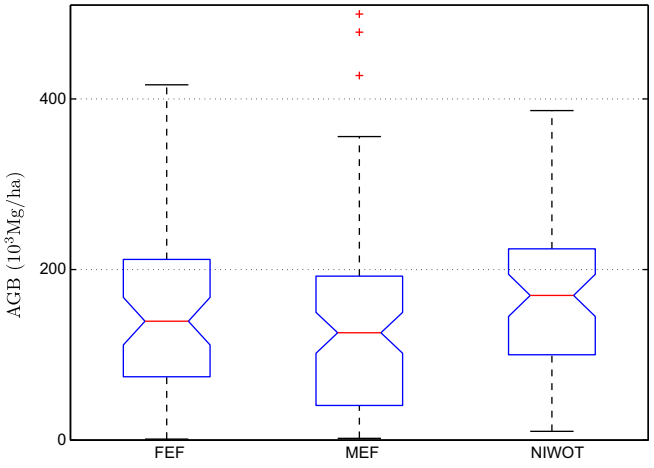

Fig. 1. Boxplots of AGB of distribution in given test sites. Median, 25th and 75th percentiles and outliers are shown.

in given test sites is shown in Fig. 1. Prior to analysis, each plot's AGB measurements were square root transformed to better approximate a normal distribution which is more likely to produce good predictions in terms of the given normality assumptions of the model residual. This variable, $\widetilde{\text{AGB}}$, serves as the response in (1).

LiDAR point return density profiles were constructed for each plot by summing the number of returns within 1 m height bins over the given plot. LiDAR returns within the 0–1 m height class were removed to limit the influence of low vegetation and local topographic features. To correct for variation in the number of returns, due to flight path overlap and laser scan angle, each profile was normalized by dividing each bin count by the maximum bin count.

LiDAR profiles were partitioned into 10th, 20th, 25th, 30th, 40th, 50th, 60th, 70th, 75th, 80th, 90th, 95th and 100th height percentiles, and stored in a $N \times 13$ matrix $\boldsymbol{Z}$ where rows correspond to plots and columns holds percentile heights. Several studies, some noted in Section 1, have shown that variables in $\boldsymbol{Z}$ are useful for explaining the variability in AGB. However, due to high collinearity among the columns, this entire matrix cannot be used as the design matrix in (1). Rather, we used a singular value decomposition (SVD) to extract the maximum information from $\boldsymbol{Z}$ using the fewest number of variables.

Prior to decomposition, each column of $\boldsymbol{Z}$ was scaled to have a mean of zero and unit variance. Then we decomposed the $N \times m$ matrix $\boldsymbol{Z} = \boldsymbol{U}\boldsymbol{\Lambda}\boldsymbol{V}'$, where the orthogonal matrices $\boldsymbol{U}$ and $\boldsymbol{V}$ are $N \times N$ and $m \times m$, respectively. The columns of $\boldsymbol{U}$ and $\boldsymbol{V}$ are often called the left and right singular vectors. The diagonal values of $N \times m$ matrix $\boldsymbol{\Lambda}$ contain the singular values (square root of eigenvalues of $\boldsymbol{Z}'\boldsymbol{Z}$ and $\boldsymbol{Z}\boldsymbol{Z}'$) in decreasing order corresponding to the columns in matrices $\boldsymbol{U}$ and $\boldsymbol{V}$, other components in the matrix are zero. In practice, a subset of columns from $\boldsymbol{U}\boldsymbol{\Lambda}$ (i.e., principal component scores) can be used as variables in regression analysis – referred to as principal components regression (Chatterjee and Hadi, 2006). Thus the columns of $\boldsymbol{U}\boldsymbol{\Lambda}$ represent the new, orthogonal, candidate set of covariates. Those components that correspond to the eigenvalues which explain 90%, of the data are used for $\boldsymbol{X}$. That is, the eigenvectors corresponding to the p largest eigenvalues, such that 90% of the variability of the data is explained, were used as covariates in the subsequent analyses. To meet the 90% criteria 6, 7, and 9 eigenvectors were needed for FEF, MEF, and NIWOT, respectively. Finally, to facilitate interpretation, the p columns of each sites' $\boldsymbol{X}$ were scaled to range from $[-1, 1]$. Both the 90% of variance explained and scaling bounds were chosen somewhat arbitrarily, but are reasonable for our subsequent analyses.

3.2. Analysis and assessment

Using the data detailed in Section 3.1 and design criteria in Section 2.1 we considered the following six designs: Maximin based on geographic coordinates, $u_{m,\boldsymbol{S}}(\boldsymbol{f})$ labeled $\text{MM}_{\boldsymbol{S}}$; Maximin based on feature space coordinates defined by $\boldsymbol{X}$, $u_{m,\boldsymbol{X}}(\boldsymbol{f})$, labeled $\text{MM}_{\boldsymbol{X}}$, and; minimization of linear prediction variance, $u_{\text{lin},\boldsymbol{\theta}}(\boldsymbol{f})$ with $\boldsymbol{\theta} = \{\tau^2, \sigma^2, \phi\}$ equal to $\{0, 1, -ln(0.05)/(r*d_{max}))\}$, where $r = \{0.1, 0.5, 0.9\}$ and d_{max} is the maximum Euclidean distance between any two plots in the sites. Recall, we are working with the Exponential correlation function; therefore, r determines the effective spatial range, i.e., 10, 50, and 90 percent of d_{max}. Therefore, the four linear prediction variance criteria are labeled LPV_{10}, LPV_{50}, and LPV_{90} for 10, 50, and 90 percent of d_{max}, respectively. We also considered the aspatial case where $u_{\text{lin},\boldsymbol{\theta}}(\boldsymbol{f})$ is equal to (9), and label this design LPV_0 where the subscript reminds us that residual spatial correlation is assumed to be zero.

Note, for LPV_{10}, LPV_{50}, and LPV_{90}, the values of ϕ in $\boldsymbol{\theta}$ will change according to the site's d_{max}. For example, say $d_{max} = 100$, then $u_{\text{lin},\boldsymbol{\theta}}(\boldsymbol{f})$ will be evaluated using ϕ values of 0.3, 0.06, and 0.03 which correspond to effective spatial ranges of 10, 50, and 90 distance units, respectively. In this way, we can explore the influence of residual spatial dependence on the sample selection.

For each of the six designs, we vary the number of possible n from 10 to 50, 90, and 60, for FEF, MEF, and NIWOT, respectively. In practice, N would be the number of fixed area plots that comprise the *a priori* unobserved inventory population. However, to assess the design criteria, we treat the observed plots as our sample frame.

As noted in Section 1, the different designs are assessed based on predictive ability and bias. To do this we perform a Leave-One-Out (LOO) cross-validation. For a given site, the LOO steps are as follows: (1) holdout the ith plot from the sample frame; (2) determine the optimal sample $\boldsymbol{f}$ from the sample frame of $N-1$ plots according to the given design and n; (3) estimate the parameters in (1) using the data from the sample and predict $\widetilde{\text{AGB}}$ for the ith holdout plot; (4) repeat steps 1–3 for all i in $1, \ldots, N$. This procedure results in N predicted values of $\widetilde{\text{AGB}}$, i.e., $\hat{\boldsymbol{y}} = (\hat{y}_1, \hat{y}_2, \ldots, \hat{y}_N)'$ obtained using the posterior predictive distribution defined in Section 2, that can be compared to their corresponding observed values. Additionally, we obtain a *baseline* prediction of $\widetilde{\text{AGB}}$ using the above LOO procedure but use the entire sample frame in step 2, i.e., setting $n = N-1$ uses all available information to estimate the model parameters and subsequent prediction of the given holdout plot. Predicted $\widetilde{\text{AGB}}$ values resulting from the design criteria and baseline LOO cross-validations were assessed using the relative root mean square error RMSE%,

$$\text{RMSE}\% = \frac{\sqrt{\sum_{i=1}^{N}(\hat{y}_i - y_i)^2/N}}{\bar{\boldsymbol{y}}} \tag{10}$$

and relative estimated bias, Bias%,

$$\text{Bias}\% = \frac{\sum_{i=1}^{N}(\hat{y}_i - y_i)/N}{\bar{\boldsymbol{y}}}, \tag{11}$$

where $\bar{\boldsymbol{y}} = \sum_{i=1}^{N}\boldsymbol{y}_i/N$. Field plots have been collected with a systematic or random sampling design. Therefore the difference between the mean value of a forest variable measured from sample plots and that measured from the corresponding model forecasts can be used to estimate model bias, down to respective sampling error.

4. Results and discussion

Application of the different design criteria results in selection of different plots into the sample. Visualizing the distribution of sample plots in a given feature space is helpful for understanding how the criteria sample from the sample frame. For example, Figs. 2 and 3 illustrate FEF's $n = 12$ sample solutions. Here, Fig. 2a and d shows the distribution of samples in geographic and covariate space, respectively, using $\text{MM}_{\boldsymbol{S}}$. Give the nearly even distribution in Sub-Fig. 2a versus the seemingly random distribution in 2d, it is clear $\text{MM}_{\boldsymbol{S}}$ seeks to cover geographic space. In contrast, $\text{MM}_{\boldsymbol{X}}$ attempts to cover covariate space, Sub-Fig. 2e, opposed to geographic space Sub-Fig. 2b. Note, for brevity we are only displaying the space defined by the first two covariate columns of $\boldsymbol{X}$, which correspond to the two largest singular values. The linear predictive variance designs do something quite different than the Maximin designs. When the effective spatial range is assumed to be zero or negligible, i.e., no or little spatial dependence among the model residuals, the LPV criteria select samples on and near the covariate space convex hull. This can be seen in the LPV_0 solution illustrated in Sub-Fig. 2f.

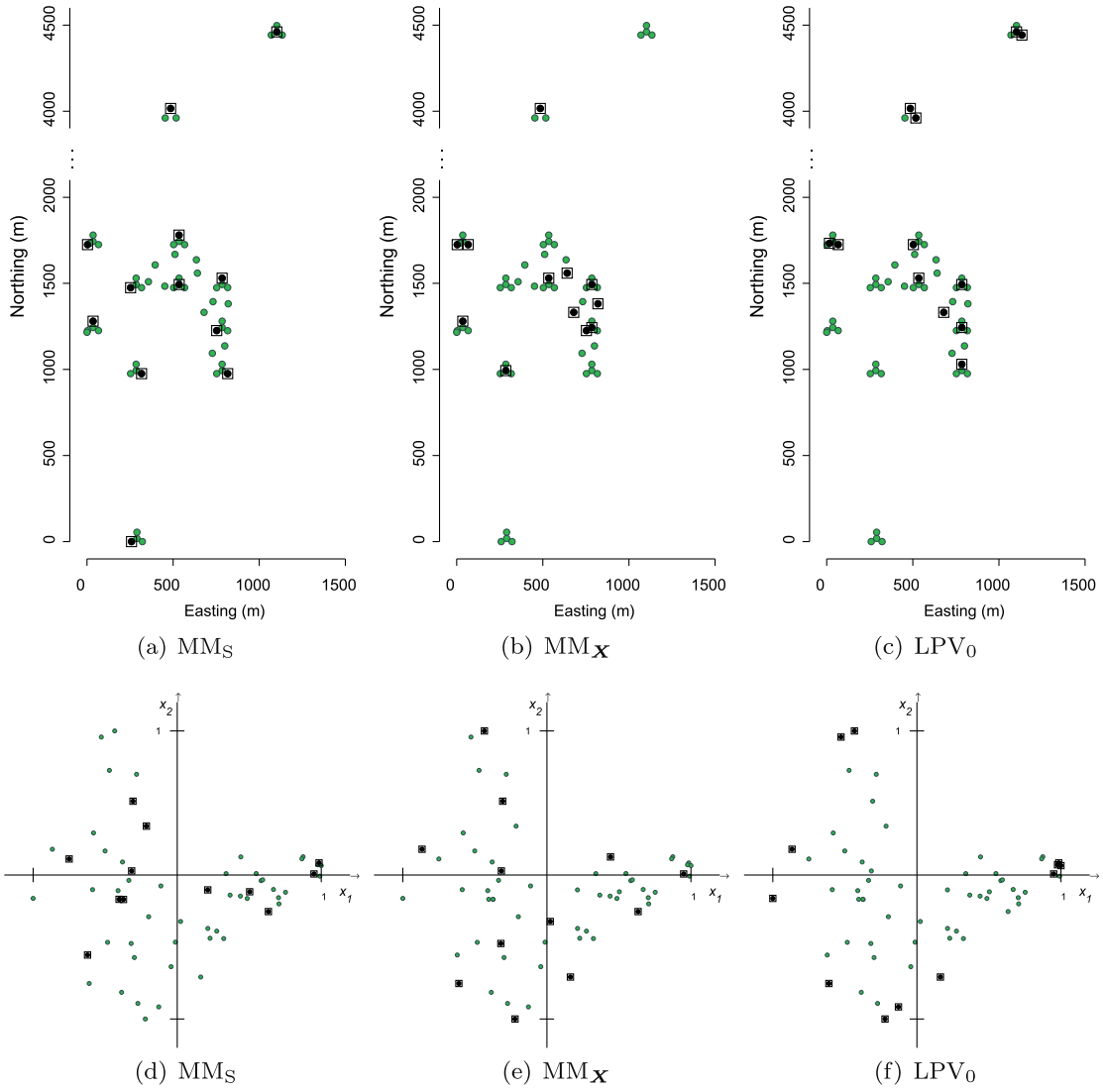

Fig. 2. Distribution of Fraser Experimental Forest (FEF) sample frame, plots denoted with circle symbols, in geographic and covariate feature space, top and bottom rows respectively. Square symbols indicate those plots selected into the $n = 12$ sample using MM$_S$, MM$_X$, and LPV$_0$ design criteria.

Designs LPV$_{10}$, LPV$_{50}$, and LPV$_{90}$ assume an increasing range of residual spatial dependence. Despite the disparity in assumed effective spatial range for FEF, i.e., 10% (448 m), 50% (2240 m), 90% (4030 m), all of these designs result in relatively even coverage in both geographic and covariate space as illustrated in Fig. 3. Although not presented, results for MEF and NIWOT show similar sample plot patterns for the design criteria.

Although not apparent in these figures, increasing the assumed spatial range should result in a more over-dispersed coverage in geographic feature space versus covariate feature space. To understand this better, consider minimizing the first component in the utility function, i.e., (6), which affects the plot selection in such a manner that plots located close to each other in geographic space are not included, while also preferentially selecting plots in proximity to plots in $\boldsymbol{v}$, i.e., presumably those locations where we will want to make a prediction. To see the effect of minimizing the second component, (7), it is useful to consider its parts: the first, $\left(\boldsymbol{X}_{\boldsymbol{f}}'\boldsymbol{\Sigma}_{\boldsymbol{f}}(\boldsymbol{\theta})^{-1}\boldsymbol{X}_{\boldsymbol{f}}\right)$, affects the plot selection in a manner similar to LPV$_0$, with the addition that plots proximate to each other in geographic space are not included in the sample if their covariate values are similar. The influence of this part depends on the covariance parameters. The second, rows in $\boldsymbol{\Delta x_v}$, appear in the form of squared values in the utility function, so that their optimal value is zero. The minimum is reached when covariate values of each verification plot $j \in \boldsymbol{v}$ can be estimated as the weighted average of the covariate values of the sample plots located within the effective spatial range from the verification plot, $\boldsymbol{x}_j \simeq \boldsymbol{c}_j(\boldsymbol{\eta})'\boldsymbol{\Sigma}_{\boldsymbol{f}}(\boldsymbol{\theta})^{-1}\boldsymbol{X}_{\boldsymbol{f}}$. If weak spatial correlation is assumed, the second component of the utility function, (7), leads to designs close to that of LPV$_0$. With stronger spatial correlation, the covariate values in the verification plots are explained more and more with covariate values of their nearest spatial neighbors. The resulting design, summation of the two components, Eq. (5), is a combination of these features.

Alternative plot layout designs had only minimal impact on predictive performance in the three forested landscapes examined here. The predictive performance of the design criteria compared to that of the baseline is provided in Figs. 4–6 for FEF, MEF, and NIWOT, respectively. For all sites, the Bias% and RMSE% results are similar among different designs – converging toward the baseline as n increases.

These results provide insight about how sampling intensity influences bias and RMSE of resulting predictions. For FEF and MEF, a Bias% within ±3% of the baseline is consistently obtained beyond $n \approx 25$ and $n \approx 35$, respectfully, for all designs except MM$_S$

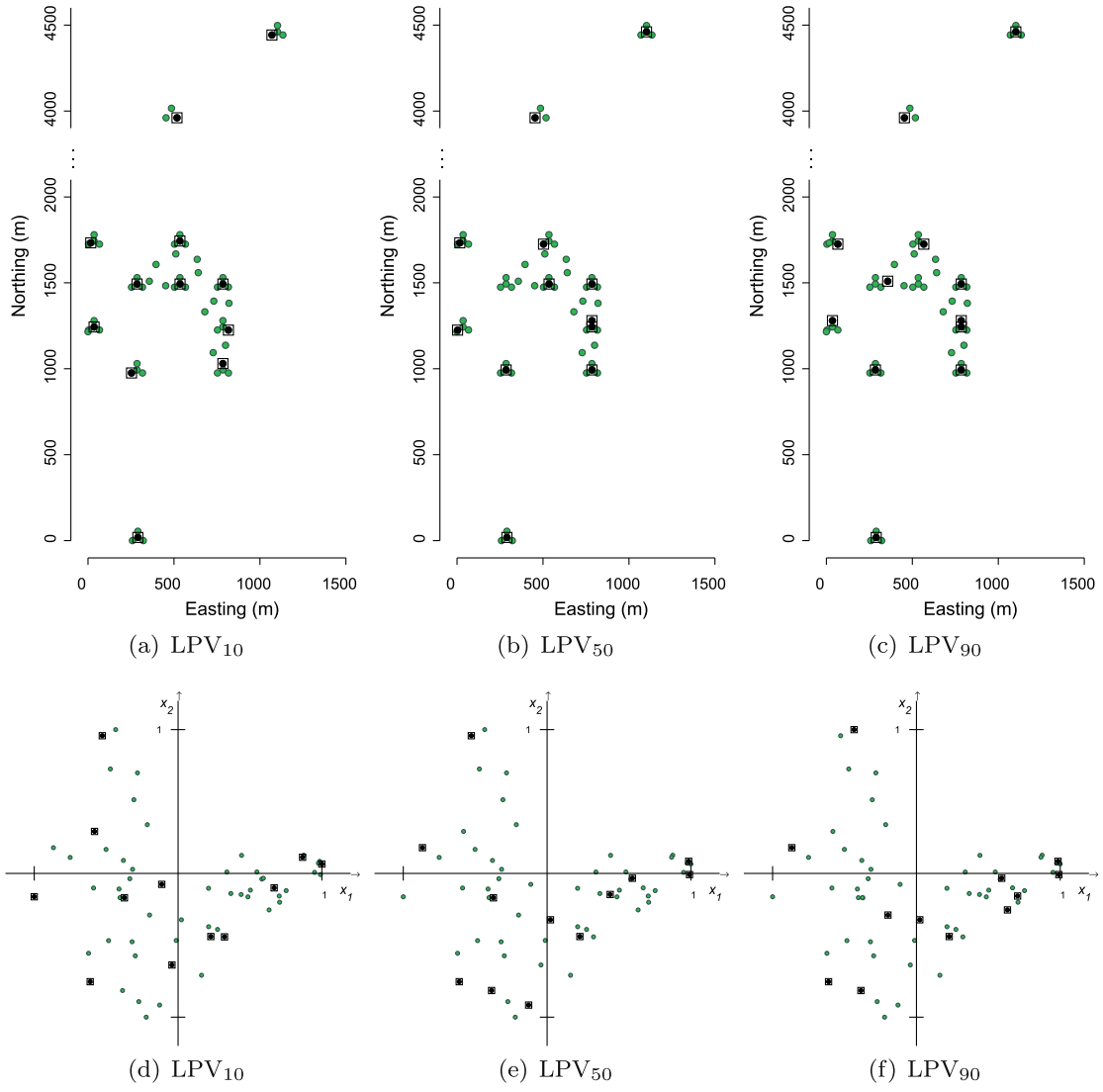

Fig. 3. Distribution of Fraser Experimental Forest (FEF) sample frame, plots denoted with circle symbols, in geographic and covariate feature space, top and bottom rows respectively. Square symbols indicate those plots selected into the $n = 12$ sample using LPV_{10}, LPV_{50}, and LPV_{90} design criteria.

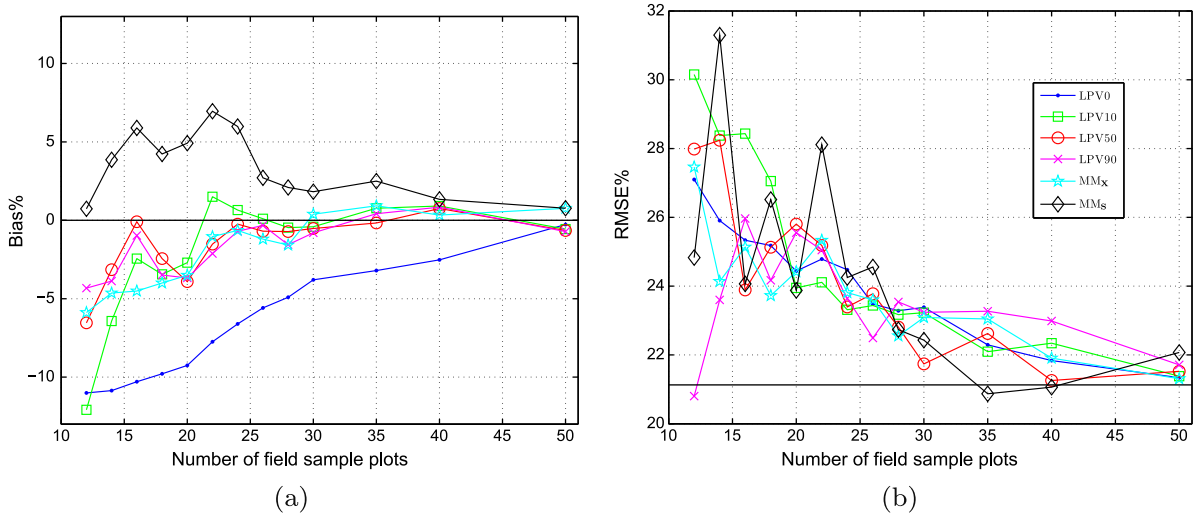

Fig. 4. Fraser Experimental Forest (FEF) design criteria and baseline (solid horizontal line) prediction Bias% (left) and RMSE% (right) for sample size n.

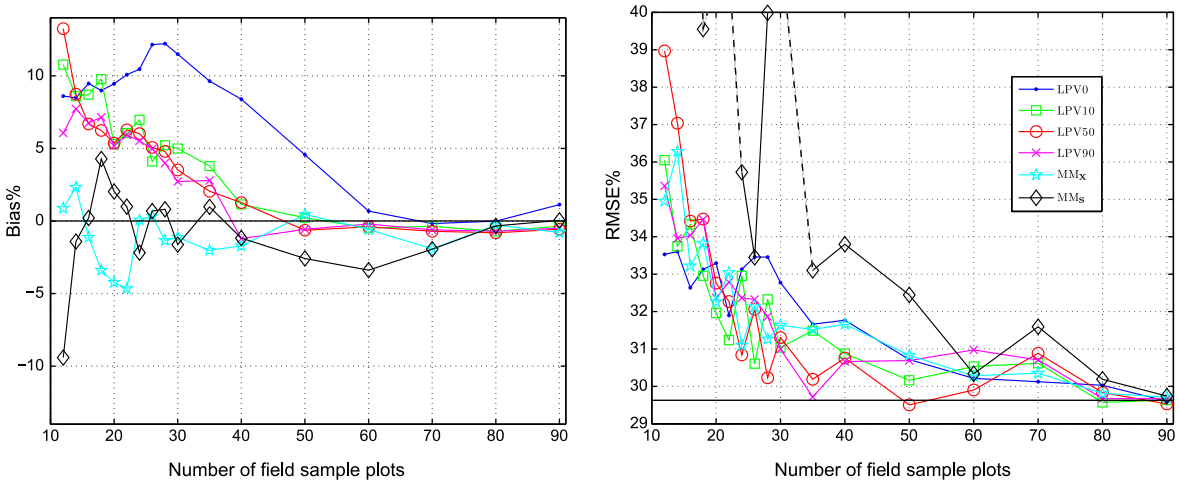

Fig. 5. Marcell Experimental Forest (MEF) design criteria and baseline (solid horizontal line) prediction Bias% (left) and RMSE% (right) for sample size n.

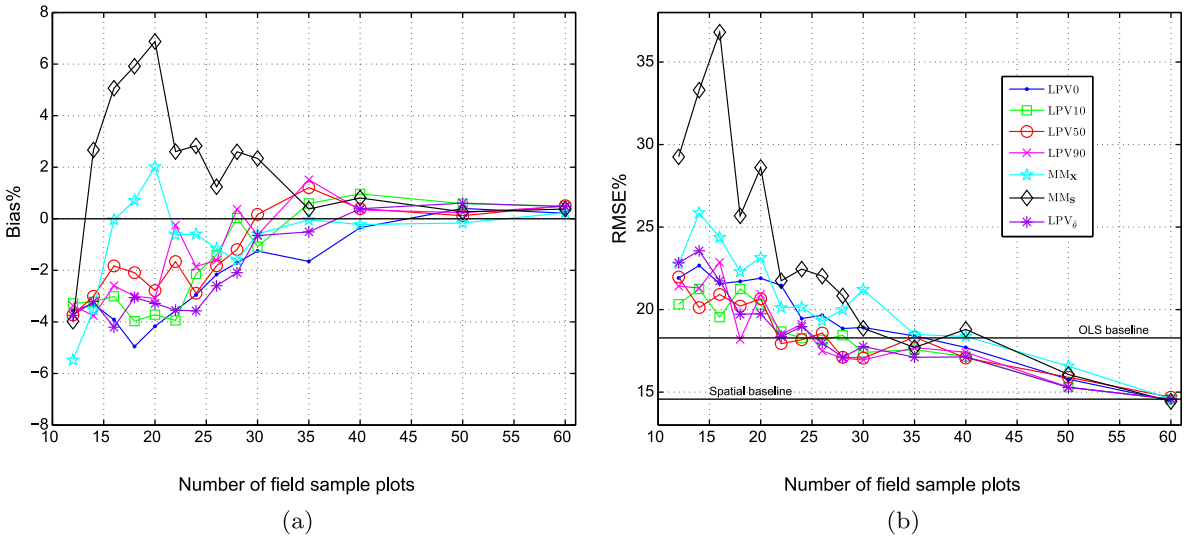

Fig. 6. Niwot Long Term Ecological Research Site (NIWOT) design criteria and baseline (solid horizontal line) prediction Bias% (left) and RMSE% (right) for sample size n.

and LPV_0. For NIWOT, all designs achieve a Bias% within ±3% of the baseline beyond $n \approx 35$. The LPV_0 Bias% for FEF and MEF deviates substantially from the other designs and baseline. This design preferentially selects sample plots at the extremes of the covariates' ranges which can result in a response vector $\boldsymbol{y}_{\boldsymbol{f}^*}$ that is not representative of the verification plots' response values and hence strongly biased prediction. This bias can be exacerbated as p increases and when the correlation between covariates and the response variable is strong. In contrast, the LPV_{10}, LPV_{50}, LPV_{90} designs provide a more representative sample and hence lower predictive bias by forcing some degree of coverage in both geographic and covariate space, as illustrated in Fig. 3. Visualization of the design LPV_{50} with $n = 20$ for each test site is given in Figs. 7–9.

Across all three sites, the $MM_{\boldsymbol{x}}$, LPV_{10}, LPV_{50}, LPV_{90} designs maintain low Bias% and RMSE% beyond a sample size of ≈35 compared to the other designs. For NIWOT, $MM_{\boldsymbol{x}}$ shows slightly higher RMSE% compared to that achieved by LPV_{10}, LPV_{50}, LPV_{90}, suggesting a spatial structure in AGB that, when incorporated into sample plot design, may enhance predictions. Because we do not know $\boldsymbol{\theta}$ *a priori*, the $u_{\text{lin},\boldsymbol{\theta}}(\boldsymbol{f})$ designs must use some reasonable estimate of τ^2, σ^2, and ϕ. Here we considered a range of values for ϕ, all of which resulted in comparable predictive performance. But how different would our results be if the *true* value of $\boldsymbol{\theta}$ was used? As an exploratory analysis, we used all data to fit site-specific non-spatial ordinary least squares (OLS) regression models that included the LiDAR covariates. Then we fit semivariograms to the models' residuals (plots not shown). The FEF and MEF semivariograms revealed no spatial structure, i.e., the LiDAR covariates explain the majority of the spatial pattern in AGB. Hence, we would not expect much difference between the results of a baseline model with or without spatial random effects. This too explains why $MM_{\boldsymbol{x}}$ performs as well as LPV_{10}, LPV_{50}, LPV_{90}. On the other hand, the semivariogram for NIWOT showed moderately strong spatial structure, i.e., the LiDAR covariates do not explain all of the spatial pattern in AGB and therefore gains in predictive performance should be realized by adding spatial random effects. These gains can be seen in Sub-Fig. 6b, which includes the baseline RMSE% achieved using the OLS (18.3%) and regression model with spatial random effects (14.6%). The need for spatial random effects in the regression model for NIWOT also helps to explain why LPV_{10}, LPV_{50}, LPV_{90} produce marginally lower RMSE% compared to that of $MM_{\boldsymbol{x}}$. Lastly, Fig. 6

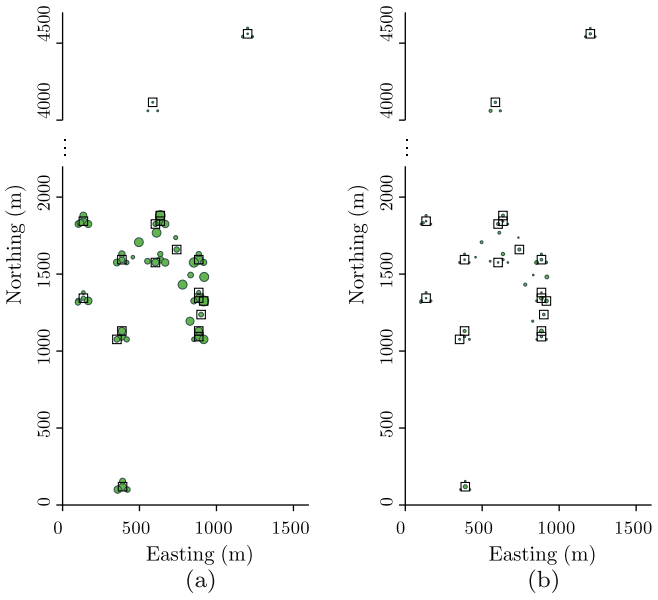

Fig. 7. 20 Field sample plots (shown with black squares) selected with the LPV_{50} design in test site FEF. On the left, the field sample measurements, on the right, the absolute errors of the estimates. The size of the circle represents the amount of plot level AGB or error, in the same scale.

includes an additional line, labeled $LVP_{\hat{\theta}}$ that uses the $\hat{\boldsymbol{\theta}}$ estimated from NIWOT's semivariogram using all the 62 plots. Importantly, this line does not deviate much from the those of LPV_{10}, LPV_{50}, LPV_{90}, which suggests that the design is robust to moderate misspecification of $\boldsymbol{\theta}$.

5. Summary

Given the case study results, we again consider our initial questions. *First, can we realize gains in efficiency when the postulated model is considered in the plot selection?* Here, a linear regression with spatial random effects served as our postulated model. Lack of residual spatial dependence, i.e., after considering the LiDAR covariates, among the plot measurements reduced the impact of the spatial random effects at the FEF and MEF sites. However, given the residual spatial pattern at NIWOT, the addition of the random effects did influence the design and hence improved prediction – albeit to a small degree. Regardless, of the presence of residual spatial dependence, those LPV designs that forced coverage in both covariate and geographic feature space yielded designs that resulted in better predictive performance than designs that sought coverage in only geographic space or at the extremes of the covariate space, i.e., $MM_{\boldsymbol{S}}$ and LPV_0 respectively. In fact, our results showed that LPV_0 and, to a lesser degree, $MM_{\boldsymbol{S}}$ can result in large prediction bias relative to other designs and should probabily not be used in practice.

Second, can we use a priori knowledge about a possible relationship between LiDAR covariates and the forest response variable to preferentially select plot locations to sample? In this study, the *a priori* information comes in several forms. For instance, based on results from previous studies, we assumed there was at least a moderately strong relationship between AGB and the set of LiDAR covariates that explained a large portion of variability in the LiDAR signal – likely covariates associated with canopy height and other biophysical canopy characteristics. Also, based on these prior studies, we assumed the relationship between AGB and LiDAR covariates could be cast as a linear model. Finally, the geographic extent of the different sites helped, to some degree, in determining reasonable support for the spatial range parameter ϕ. In practice, we could garner

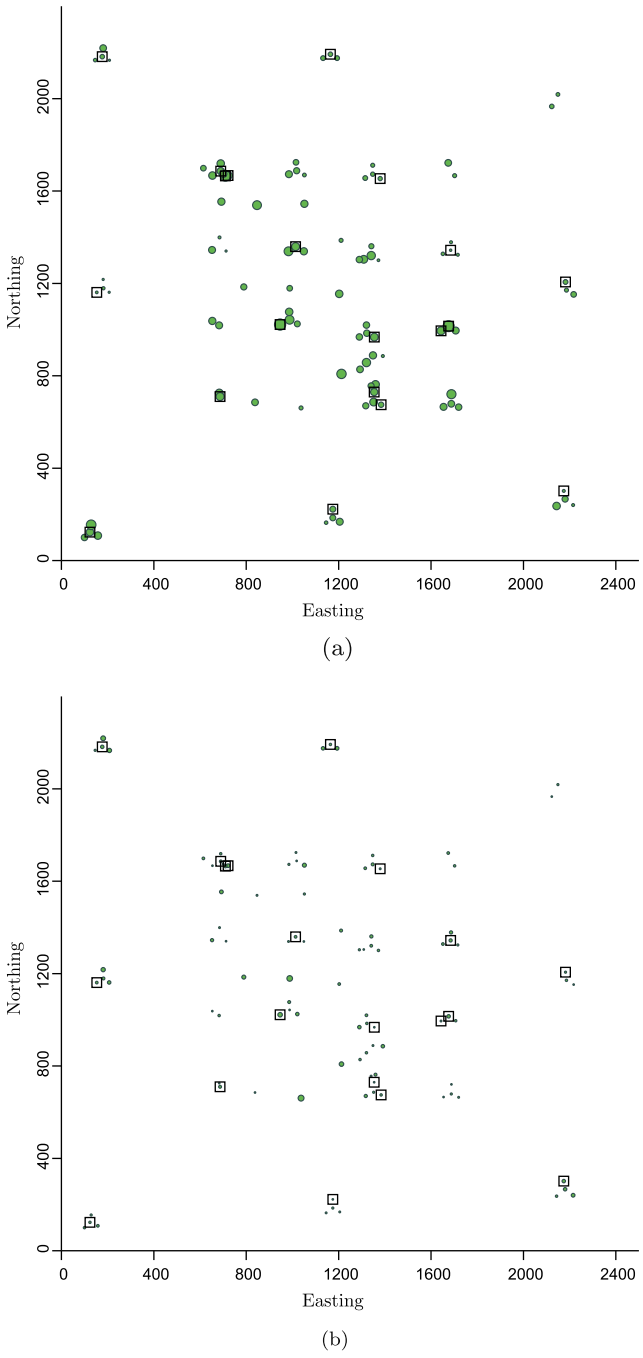

Fig. 8. 20 Field sample plots (shown with black squares) selected with the LPV_{50} design in test site MEF. On the top, the field sample measurements, on the bottom, the absolute errors of the estimates. The size of the circle represents the amount of plot level AGB or error, in the same scale.

additional information from modeling exercises conducted at similar sites. This additional information could include specific LiDAR covariates, e.g., those corresponding to specific crown and/or stand characteristics, distribution of the regression parameter's that could inform prior distributions at new sites, and better initial estimates of $\boldsymbol{\theta}$. However, our results suggest that the LPV design solution is fairly robust to misspecification of $\boldsymbol{\theta}$.

Third, are the answers to the first and second questions consistent across sites? As noted previously, presence of residual spatial dependence does influence the design. Given our postulated model, stronger residual spatial dependence should result in greater

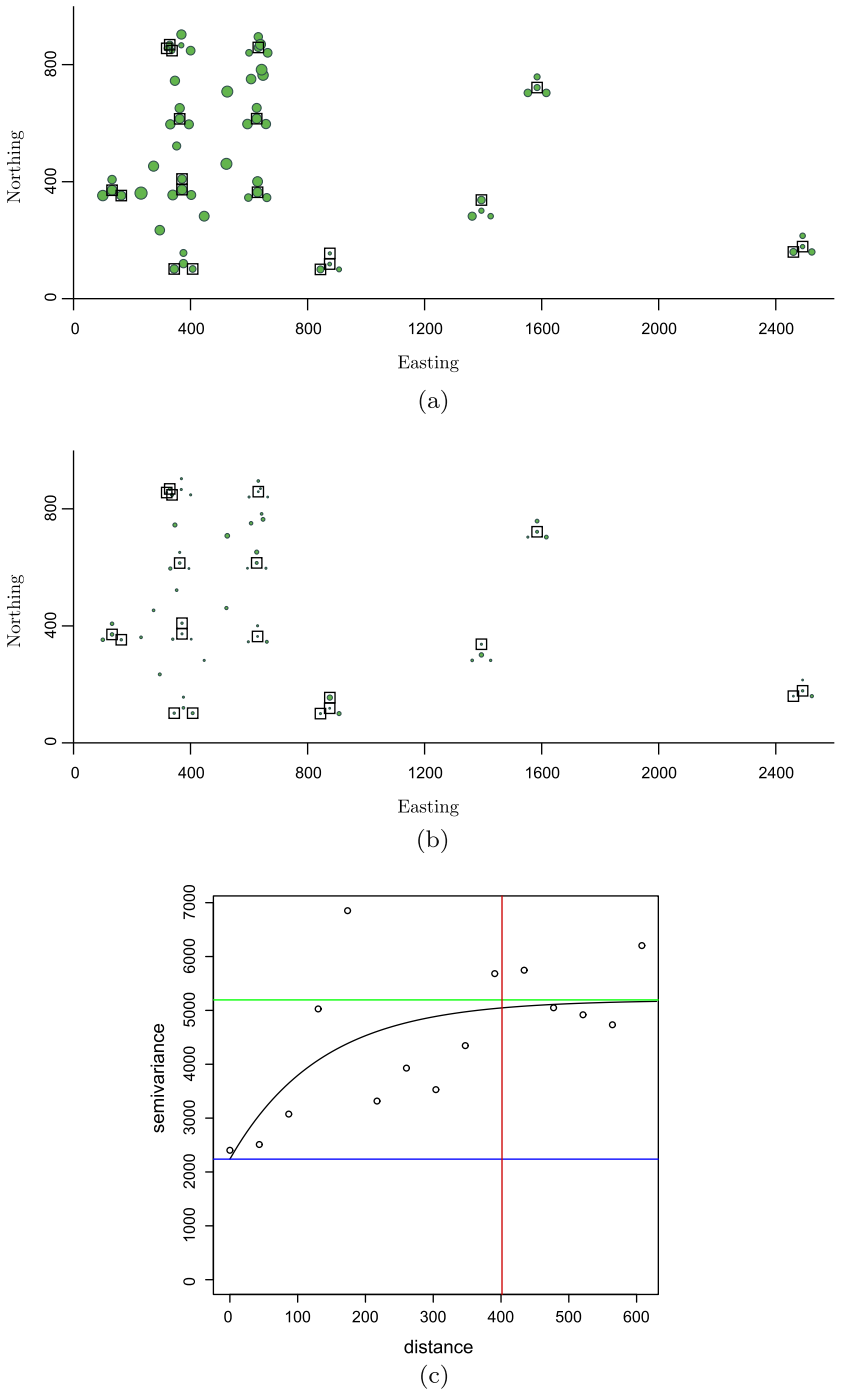

Fig. 9. On the top and middle: 20 field sample plots (shown with black squares) selected with the LPV_{50} design in test site NIWOT. On the top, the field sample measurements, in the middle, the absolute errors of the estimates. The size of the circle represents the amount of plot level AGB or error, in the same scale. On the bottom: The semivariogram of the model residuals.

gains in predictive performance. Also, the results suggest that $MM_{\boldsymbol{x}}$ and those LPV_0 designs that acknowledge some degree of residual spatial dependence do perform similarly across the three sites. Across sites, use of the $MM_{\boldsymbol{x}}$ or the spatial LPV designs allow the number of plots to be reduced by approximately 20 with marginal impact on RMSE or bias.

From a practical point-of-view in conducting medium-scale forest inventory campaigns that use airborne LiDAR, it can be concluded that just about forty field plots can be enough to calibrate an accurate and precise linear regression model for estimating above-ground biomass, based on LiDAR covariates. Selecting these forty plots so that they span very well the variability of forest features present in the target forest, and adequately well also the spatial extent of the forest, appears sufficient for robust estimation results. Several plot selection criteria suitable for this purpose were identified and compared. The strength of the conclusions obtained is limited to some extent by the smallish number of sample plots available from our case study sites, and this should therefore be taken as a caveat to their validity.

Acknowledgments

The work of the second author was supported by the USDA Forest Service, Forest Inventory and Analysis National Program, Forest

Health Technology Enterprise Team, and National Science Foundation (NSF) Grants EF-1137309 and NSF-DMS-1106609. The three authors were supported by USDA/NASA grant 10-JV-11242307-037. The first two authors were supported by NASA Carbon Monitoring System grants 11-CMS11-0021 and 11-CMS11-0028.

Significant funding for collection of these data was provided by the U.S. Forest Service. Any use of trade, product, or firm names is for descriptive purposes only and does not imply endorsement by the U.S. Government.

References

Atkinson, A.C., Donev, A.N., 1992. Optimum Experimental Designs. Oxford University Press.

Banerjee, S., Carlin, B., Gelfand, A., 2004. Hierarchical Modeling and Analysis for Spatial Data. Chapman & Hall.

Bechtold, W., Patterson, P., 2005. The enhanced forest inventory and analysis program – national sampling design and estimation procedures. General Technical Report SRS-80. USDA Forest Service, Southern Research Station 85, Asheville, NC, USA.

Bradford, J.B., Weishampel, P., Smith, M.-L., Kolka, R., Birdsey, R.A., Ollinger, S.V., Ryan, M.G., 2010. Carbon pools and fluxes in small temperate forest landscapes: variability and implications for sampling design. Forest Ecology and Management 259, 1245–1254.

Brown, S., 2002. Measuring carbon in forests: current status and future challenges. Environmental Pollution 116, 363–372.

Brus, D.J., Heuvelink, G.B.M., 2007. Optimization of sample patterns for universal kriging of environmental variables. Geoderma 138, 86–95.

Chatterjee, S., Hadi, A.S., 2006. Regression Analysis by Example. John Wiley & Sons, Inc.

Chilés, J.P., Delfiner, P., 1999. Geostatistics: Modeling Spatial Uncertainty. Wiley, New York.

Christensen, R., 1990. Linear Models for Multivariate, Time Series and Spatial Data. Springer, New York.

Cressie, N.A.C., 1993. Statistics for Spatial Data. Wiley, New York.

Fang, Z., Wiens, D., 2000. Integer-valued minimax robust designs for estimation in heteroscedastic, approximately linear models. Journal of American Statistical Association 95 (451), 807–818.

Finley, A.O., Banerjee, S., 2012. Point-Referenced Spatial Modeling, the SAGE Handbook of Multilevel Modeling. Sage Publishing., In press.

Finley, A.O., Banerjee, S., Ek, A.R., McRoberts, R.E., 2008a. Bayesian multivariate process modeling for prediction of forest attributes. Journal of Agricultural, Biological, and Environmental Statistics 13, 60–83.

Finley, A.O., Banerjee, S., MacFarlane, D.W., 2011. A hierarchical model for quantifying forest variables over large heterogeneous landscapes with uncertain forest areas. Journal of the American Statistical Association 106, 31–48.

Finley, A.O., Banerjee, S., McRoberts, R.E., 2008b. A bayesian approach to quantifying uncertainty in multi-source forest area estimates. Environmental and Ecological Statistics 15, 241–258.

Finley, A.O., Banerjee, S., McRoberts, R.E., 2009. Hierarchical spatial models for predicting tree species assemblages across large domains. Annals of Applied Statistics 3, 1052–1079.

Hawbaker, T.J., Keuler, N.S., Lesak, A.A., Gobakken, T., Contrucci, K., 2009. Improved estimates of forest vegetation structure and biomass with a lidar-optimized sampling design. Journal of Geophysical Research 114, 11.

Hengl, T., Rossiter, D., Stein, A., 2003. Soil sampling strategies for spatial prediction by correlation with auxiliary maps. Australian Journal of Soil Research 41, 1403–1422.

Hudak, A.T., Lefsky, M.A., Cohen, W.B., Berterretche, M., 2002. Integration of lidar and landsat etm+ data for estimating and mapping forest canopy height. Remote Sensing of Environment 82, 397–416.

Junttila, V., Maltamo, M., Kauranne, T., 2008. Sparse Bayesian estimation of forest stand characteristics from airborne laser scanning. Forest Science 54 (5), 543–552.

Magnussen, S., Næsset, E., Gobakken, T., 2010. Reliability of lidar derived predictors of forest inventory attributes: a case study with norway spruce. Remote Sensing of Environment 114, 700–712.

Maltamo, M., Bollandsås, O.M., Næsset, E., Gobakken, T., Packalén, P., 2011a. Different plot selection strategies for field training data in ALS-assisted forest inventory. Forestry 84 (1), 23–31.

Maltamo, M., Packalén, P., Kallio, E., Kangas, J., Uuttera, J., Heikkilä, J., 2011b. Airborne laser scanning based stand level management inventory in finland. In: Proceedings of SilviLaser 2011, 11th International Conference on LiDAR Applications for Assessing Forest Ecosystems, University of Tasmania, Australia, 16–20 October 2011. pp. 1–10.

McRoberts, R.E., 2012. Estimating forest attribute parameters for small areas using nearest neighbors techniques. Forest Ecology and Management 272, 3–12.

McRoberts, R.E., Bechtold, W.A., Patterson, P.L., Scott, C.T., Reams, G.A., 2005. The enhanced forest inventory and analysis program of the usda forest service: Historical perspective and announcement of statistical documentation. Journal of Forestry 103 (6), 304–308.

Means, J.E., Acker, S.A., Harding, D.J., Blair, J.B., Lefsky, M.A., Cohen, W.B., Harmon, M.E., McKee, W.A., 1999. Use of large-footprint scanning airborne lidar to estimate forest stand characteristics in the western cascades of oregon. Remote Sensing of Environment 67, 298–308.

Morris, M.D., Mitchell, T.J., 1995. Exploratory designs for computational experiments. Journal of Statistical Planning and Inference 43 (3), 381–402.

Næsset, E., 1997. Determination of mean tree height of forest stands using airborne laser scanning data. ISPR Journal of Photogrammetry and Remote Sensing 52 (2), 49–56.

Paciomik, N., Rypdal, K., 2003. Good practice guidance for land use, land-use change and forestry, intergovernmental panel on climate change national greenhouse gas inventories programme. In: Penman, J., Gytartsky, M., Hiraishi, T., Krug, T., Kruger, D., Pipatti, R., Buendia, L., Miwa, K., Ngara, T., Tanabe, K., Wagner, F. (Eds.), Cross cutting issues. Institute for Global Environmental Strategies (IGES), Kanagawa, pp. 5.21–5.28 (Chapter section 5.3 sampling).

Patenaude, G., Hill, R.A., Milne, R., Gaveau, D.L.A., Briggs, B.B.J., Dawson, T.P., 2004. Quantifying forest above ground carbon content using lidar remote sensing. Remote Sensing of Environment 93 (3), 368–380.

Rooker Jensen, J.L., Humes, K.S., Conner, T., Williams, C.J., DeGroot, J., 2006. Estimation of biophysical characteristics for highly variable mixed-conifer stands using small-footprint lidar. Canadian Journal of Forest Research 36, 1129–1138.

Silvey, S.D., 1980. Optimal Design. Chapman and Hall.

Trosset, M., 1999. Approximate maximin distance designs. In: Proceedings of the Section on Physical and Engineering Sciences. American Statistical Association, pp. 223–227.

Zhou, J., 2008. D-optimal minimax regression designs on discrete design space. Journal of Statistical Planning and Inference 138, 4081–4092.